First principles phase diagram calculations for the system $NaNbO_3$–$KNbO_3$: Can spinodal decomposition generate relaxor ferroelectricity?

B. P. Burton[a)]
Ceramics Division, Materials Science and Engineering Laboratory, National Institute of Standards and Technology (NIST), Gaithersburg, Maryland 20899

Takeshi Nishimatsu
Institute for Materials Research (IMR), Tohoku University, Sendai 980-8577, Japan

(Received 6 April 2007; accepted 2 August 2007; published online 27 August 2007)

First principles based phase diagram calculations were performed for the system $(1-X)$ $NaNbO_3$–(X) $KNbO_3$. Plane wave pseudopotential calculations of formation energies were used as a basis for fitting a cluster expansion Hamiltonian, and a phase diagram was calculated. The predicted phase diagram has an unusual asymmetric miscibility gap, which suggests that it might be possible to synthesize a lead-free compositionally modulated sample with bulk composition $X \approx 0.23$; such a sample is likely to exhibit relaxor characteristics. © *2007 American Institute of Physics*. [DOI: 10.1063/1.2775308]

Typically, when Na^+ and K^+ mix on the same crystallographic site of a solid solution, the system exhibits a miscibility gap: e.g., NaCl–KCl,[1,2] $NaAlSi_3O_8$–$KAlSi_3O_8$,[3] and $NaNO_3$–KNO_3,[4] $Na_3K(AlSiO_4)_4$–$K_4(AlSiO_4)_4$.[5] Hence, it seems likely that $(1-X)$ $NaNbO_3$–(X) $KNbO_3$ will also exhibit low temperature (T) immiscibility, even though it was not reported in previous studies.[6,7] Ahtee and Hewat[7] studied phase transitions below 923 K in samples that were sintered at 1323 K for 200 h, thus without slow cooling or long-term annealing, low-T immiscibility might well have escaped detection. Also, in the analogous system $(1-X)$ $NaTaO_3$–(X) $KTaO_3$, Davis[8] reports possible immiscibility in the composition range $0.16 \leqslant X \leqslant 0.26$.

Recently, there has been great interest in Pb-free piezoeletrics to replace $Pb(Zr_{1-X},Ti_X)O_3$, which is the most widely used transducer, actuator, and ferroelectric-sensor material, e.g., Refs. 9–11. Also, because of their desireable dielectric properties, there has been great interest in Pb-free relaxor ferroelectrics (relaxors), e.g., Refs. 12–15. As discussed by several authors, e.g., Refs. 16–19, relaxor characteristics arise because of local "random" fields that are caused by chemical disorder of differently charged or sized ions, or by polar defects. In $NaNbO_3$–$KNbO_3$, the different ionic sizes of Na^+ and K^+ would presumably give rise to strain mediated random fields, but the spatial average strength of these fields, $\langle h_i \rangle$ is evidently small, or conventionally prepared $(1-X)$ $NaNbO_3$–(X) $KNbO_3$ samples should exhibit relaxor properties. Immiscibility of Na- and K-rich solid solutions might, however, permit sufficient enhancement of $\langle h_i \rangle$ to induce relaxor properties; via compositional fluctuations (chemical clustering) that arise from spinodal decomposition.[20] An apparent example of relaxor-enhancement via chemical clustering is $Ba(Ti_{1-X},Zr_X)O_3$ in which x-ray absorption fine structure studies[15] indicate significant Zr-clustering in samples with $0.25 \leqslant X \leqslant 0.35$.

Formation energies ΔE_f (Fig. 1) were calculated for fully relaxed $NaNbO_3$ (20 atom cell), $KNbO_3$ (5 atom cell), and 49 $Na_mK_nNb_{(m+n)}O_{3(m+n)}$ supercells. All calculations were performed with the Vienna *ab initio* simulation program (VASP) [Version 445 (Refs. 21 and 22)] using ultrasoft Vanderbilt-type plane-wave pseudopotentials[23] with the generalized gradient approximation for exchange and correlation energies. Electronic degrees of freedom were optimized with a conjugate gradient algorithm, and both cell constant and ionic positions were fully relaxed. Pseudopotential valence electron configurations were: Na_pv $2p^6 3s^1$, K_pv $3p^6 4s^1$, Nb_pv $5s^1 4d^4$, and O_s $3s^2 3p^4$.

Total energy calculations were converged with respect to k-point meshes by using the equivalent of 6 6 6, or greater, for a five-atom $Pm\bar{3}m$ perovskite cell. A 500 eV energy cutoff was used, in the "high precision" option which guarantees that *absolute* energies are converged to within a few meV/mol (a few tenths of a kJ/mol of exchangeable cations; Na^+ or K^+; 1 mol=$Na_{1-X}K_XNbO_3$). Residual forces were typically of the order of 0.02 eV or less. To obtain fully relaxed structures, it was *not* sufficient to perform conventional relaxations without symmetry constraints. Rather,

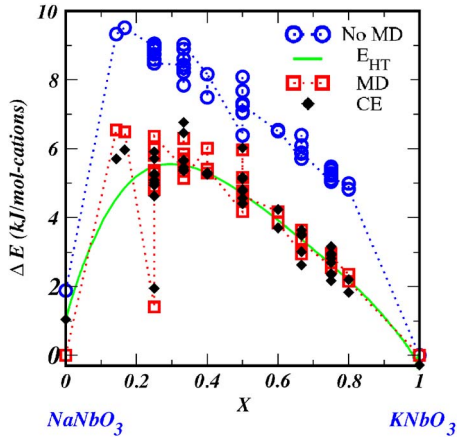

FIG. 1. (Color online) Comparison of VASP formation energies ΔE_f that were calculated by conventional 0 K relaxations (◯, "no MD") with ΔE_f from 0 K relaxations that followed 300 K annealing runs (□, "MD"). Filled diamonds (◆) indicate the cluster-expansion fit to the annealed set, and the solid curve is the high temperature cluster expansion limit for the total energy.

a)FAX: 301-975-5334; electronic mail: benjamin.burton@nist.gov

T-dependent molecular dynamics (MD) annealing, typically at 300 K, followed by normal 0 K relaxations lead to significant reductions in calculated values for ΔE_f. Performing additional annealing steps, however, never yielded significant additional reductions in ΔE_f. Figure 1 exhibits the results of conventional 0 K relaxations (○), and the 0 K relaxations that followed MD annealing (□); dotted lines are guides for the eye.

Calculated formation energies ΔE_f for 49 $Na_mK_nNb_{(m+n)}O_{3(m+n)}$ supercells are plotted in Fig. 1, where values for ΔE_f are normalized per mol of exchangeable Na^+ and K^+ ions:

$$\Delta E_f = (E_S - mE_{NaNbO_3} - nE_{KNbO_3})/(m+n). \quad (1)$$

Here, E_S is the total energy of the $Na_mK_nNb_{(m+n)}O_{3(m+n)}$ supercell, E_{NaNbO_3} is the energy/mole of $NaNbO_3$, and E_{KNbO_3} is the energy/mole of $KNbO_3$.

All supercell energies are positive which indicates a miscibility gap system.

The cluster expansion[24] (CE) is a compact representation of the configurational total energy. In the $(1-X)$ $NaNbO_3-(X)$ $KNbO_3$ quasibinary system, the solid solution configuration is described by pseudospin occupation variables σ_i, which take values $\sigma_i=-1$ when site i is occupied by Na^+ and $\sigma_i=+1$ when site i is occupied by K^+.

The CE parametrizes the configurational energy, per exchangeable cation, as a polynomial in pseudospin occupation variables

$$E(\sigma) = \sum_\ell m_\ell J_\ell \left\langle \prod_{i\in\ell'} \sigma_i \right\rangle. \quad (2)$$

Cluster ℓ is defined as a set of lattice sites. The sum is taken over all clusters ℓ that are not symmetrically equivalent in the high-T structure space group, and the average is taken over all clusters ℓ' that are symmetrically equivalent to ℓ. Coefficients J_ℓ are called effective cluster interactions (ECI) and the *multiplicity* of a cluster m_ℓ is the number of symmetrically equivalent clusters, divided by the number of cation sites. The ECI are obtained by fitting a set of VASP FP calculated structure energies $\{E_{Str}\}$. The resulting CE can be improved as necessary by increasing the number of clusters ℓ and/or the number of E_{Str} used in the fit.

Fitting was performed with the alloy theoretic automated toolkit[22,25–27] (ATAT) which automates most of the tasks associated with the construction of a CE Hamiltonian. A complete description of the algorithms underlying the code can be found in Ref. 26. The most important steps are (1) selecting which first principles (FP) structure energies to calculate, which is done in a way that minimizes the statistical variance of the estimated ECI; (2) automatically selecting which clusters to include in the expansion by minimizing the *cross-validation score* (CV),

$$(\mathrm{CV})^2 = \frac{1}{N}\sum_{\mathrm{Str}=1}^{N} (E_{Str} - \hat{E}_{Str})^2, \quad (3)$$

where $E_1,\ldots,E_N$ denote the structural energies calculated from FP and $\hat{E}_{Str}$ is the energy of structure Str *predicted* from a CE that was fit to the remaining $N-1$ energies. This criterion ensures that the chosen set of clusters maximizes the predictive power of the CE for any structure, whether or not it is included in the fit. This is an improvement relative to the standard mean square error criterion which only minimizes the error for structures that are included in the fit. The optimized cluster set, Table I, includes 12 pairs, six triplets, and three four-body terms, $CV^2=0.011$ eV. The ECIs were fitted to all 49 of the E_{Str} plotted on Fig. 1 (□), in which filled diamonds (◆) indicate ΔE_f that were calculated with the CE and the solid curve (green on line) is the high-T CE-expansion limit of the total energy. The ~1 kJ/mol overestimate of E_{NaNbO_3} suggests a small, of order 10%, underestimation of the consolute temperature T_C.

TABLE I. Effective cluster interactions in eV/mol.

Cluster coordinates minus (1,1,1)	Multiplicity m_ℓ	ECI J_ℓ (eV/cation)
Zero cluster	1	0.048604
Point cluster	1	−0.036733
(1,0,1)	3	0.002674
(0,2,1)	6	0.002150
(0,0,0)	4	−0.000911
(1,1,−1)	3	−0.003070
(1,0,−1)	12	0.000694
(2,2,3)	12	0.000012
(−1,3,1)	6	−0.000473
(1,1,−2)	3	−0.001115
(0,−1,−1)	12	−0.001186
(1,0,−2)	12	−0.001124
(0,0,−2)	12	−0.000485
(−1,−1,−1)	4	0.000789
(0,1,1), (0,2,1)	12	−0.000311
(0,1,2), (0,2,1)	8	−0.000450
(1,0,0), (0,0,0)	24	0.000628
(1,1,0), (1,1,−1)	3	0.000961
(1,0,0), (1,1,−1)	12	0.001368
(0,0,0), (1,1,−1)	12	0.000235
(1,2,2), (0,1,2), (0,2,1)	2	0.003103
(0,1,0), (1,0,0), (0,0,0)	24	−0.000773
(0,1,0), (1,0,0), (1,1,−1)	12	−0.001022

In addition to the CV-criterion, ATAT also ensures that ground states predicted from the CE agree with the minimum energy structures for each composition, as calculated from FP. The code proceeds by iterative refinement, gradually increasing the number of clusters and the number of structures to provide the best possible fit based on the current set $\{E_{Str}\}$.

First principles phase diagram (FPPD) calculations were performed with grand canonical Monte Carlo (MC) simulations using the EMC2 code which is part of the ATAT package.[25–27] Input parameters for EMC2 were a $29\times29\times29$ unit cell simulation box, 1500 equilibration passes, and 1500 Monte Carlo passes. The predicted phase diagram is shown in Fig. 2, in which, open circles indicate equilibrated MC simulations. The predicted consolute point is approximately $\{X_C,T_C\}\sim\{0.23,1720\ \mathrm{K}\}$. The dramatic asymmetry of this diagram strongly suggests short-range Na:K order based on a bulk composition near 1:1 at $T\geqslant550$ K, but attempts to identify a stable phase in this region of the $\{X,T\}$ space were unsuccessful.

Typically, FPPD calculations overestimate consolute temperatures especially when, as here, the excess vibrational contribution to the free energy is ignored. Including this con-

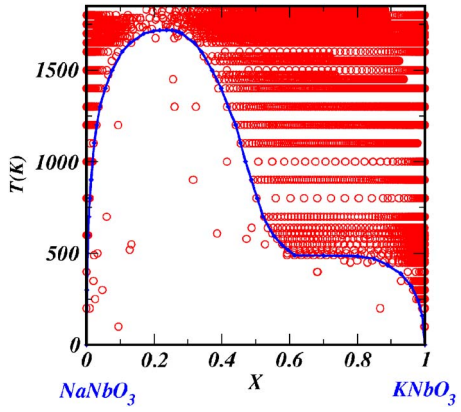

FIG. 2. (Color online) Calculated phase diagram, based on the cluster expansion that was fitted to the annealed set of formation energies (□, MD in Fig. 1). Note the unusual asymmetric miscibility gap.

tribution, however, usually leads to only a 5%–15% reduction in T_C,[28] which would not alter the conclusions of this work. The predicted miscibility gap on the Na-rich side of the $NaNbO_3$–$KNbO_3$ phase diagram suggests the possibility of synthesizing relaxor ferroelectrics by slowly cooling a sample with a bulk composition near $Na_{0.77}K_{0.23}NbO_3$. Spinodal decomposition induced Na:K concentration waves is expected to concentrate local fields in a way that promotes and enhances relaxor properties. Simulations of $Pb(Mg_{1/3}Nb_{2/3})O_3$ and $Pb(Sc_{1/2}Nb_{1/2})O_3$ (Refs. 18 and 19) indicate that chemical short-range order enhances relaxor properties, relative to a system with random chemical disorder. Similarly, x-ray absorption fine structure studies of $Ba(Ti_{1-X},Zr)_XO_3$ $(0.25 \leqslant X \leqslant 0.35)$ (Ref. 15) correlate chemical clustering of Zr with enhanced relaxor properties. Thus, it is reasonable to expect a similar effect from spinodal decomposition induced Na:K clustering in $NaNbO_3$–$KNbO_3$.

Most of the total energy calculations for this work were performed by one of the authors (B.P.B.) in the Kawazoe Laboratory of the Institute for Materials Research (IMR), Tohoku University, Sendai 980-8577, Japan while he was there as a visiting professor in 2005.

[1] J. B. Thompson and D. R. Waldbaum, Geochim. Cosmochim. Acta **33**, 671 (1969).
[2] B. P. Burton and A. van de Walle, Chem. Geol. **225**, 222 (2006).
[3] R. A. Yund and J. Tullis, *Feldspar Mineralogy: Reviews in Mineralogy*, edited by P. H. Ribbe (Mineralogical Society of America, printed by Bookcrafters, Inc., Chelsea, MI, 1983), Vol. 2, Chap. 6, p. 141.
[4] *Phase Diagrams for Ceramists*, edited by R. S. Roth, J. R. Dennis, and H. McMurdie (American Ceramic Society, Columbus, OH, 1964), Vol. VI, p. 429.
[5] J. M. Ferry and J. G. Blencoe, Am. Mineral. **63**, 1225 (1978).
[6] G. Shirane, R. Newnham, and R. Pepinsky, Phys. Rev. **96**, 581 (1954).
[7] M. Ahtee and A. W. Hewat, Acta Crystallogr., Sect. A: Cryst. Phys., Diffr., Theor. Gen. Crystallogr. **34**, 309 (1978).
[8] T. G. Davis, Phys. Rev. B **5**, 2530 (1972).
[9] P. Baettig, C. F. Schelle, R. LeSar, U. V. Waghmare, and N. Spaldin, Chem. Mater. **17**, 1376 (2005).
[10] R. E. Eitel, C. A. Randall, T. R. Shrout, P. W. Rehrig, W. Hackenberger, and S.-E. Park, Jpn. J. Appl. Phys., Part 1 **40**, 5999 (2001).
[11] J. Iniguez, D. Vanderbilt, and L. Belliache, Phys. Rev. B **67**, 224107 (2003).
[12] A. Simon, J. Ravez, and M. Maglione, J. Phys.: Condens. Matter **16**, 963 (2004).
[13] V. A. Shuvaeva, D. Zekria, A. M. Glazer, Q. Jiang, S. M. Weber, P. Bhattacharya, and P. A. Thomas, Phys. Rev. B **71**, 174114 (2005).
[14] V. Bobnar, B. Malič, J. Holc, M. Kosec, R. Steinhausen, and H. Beige, J. Appl. Phys. **98**, 024113 (2005).
[15] C. Laulhé, F. Hippert, J. Kreisel, M. Maglione, A. Simon, J. L. Hazemann, and V. Nassif, Phys. Rev. B **74**, 014106 (2006).
[16] H. Quian and L. A. Bursill, Int. J. Mod. Phys. B **10**, 2027 (1996).
[17] W. Kleemann, G. A. Samara and J. Dec, *Polar Oxides: Properties, Characterization, and Imaging*, edited by R. Waser, U. Bottger, and S. Tiedke (Wiley-VCH, Weinheim, 2005), p. 275.
[18] B. P. Burton, E. Cockayne, S. Tinte, and U. V. Waghmare, Phase Transitions **79**, 91 (2006).
[19] S. Tinte, B. P. Burton, E. Cockayne, and U. V. Waghmare, Phys. Rev. Lett. **97**, 137601 (2006).
[20] J. W. Cahn, Acta Metall. **9**, 795 (1961).
[21] G. Kresse and J. Hafner, Phys. Rev. B **47**, 558 (1993); G. Kresse, Doctoral Thesis, Technische Universität Wien, 1993; Phys. Rev. B **49**, 14251 (1994); G. Kresse and J. Furthmüller, Comput. Mater. Sci. **6**, 15 (1996); Phys. Rev. B **54**, 11169 (1996); see http://tph.tuwien.ac.at/vasp/guide/vasp.html
[22] Reference to specific software packages does not imply a NIST endorsement.
[23] D. Vanderbilt, Phys. Rev. B **41**, 7892 (1990).
[24] J. M. Sanchez, F. Ducastelle, and D. Gratias, Physica A **128A**, 334 (1984).
[25] A. van de Walle, M. Asta, and G. Ceder, CALPHAD: Comput. Coupling Phase Diagrams Thermochem. **26**, 539 (2002).
[26] A. van de Walle and G. Ceder, J. Phase Equilib. **23**, 348 (2002).
[27] A. van de Walle and M. Asta, Modell. Simul. Mater. Sci. Eng. **10**, 521 (2002).
[28] A. van de Walle and G. Ceder, Rev. Mod. Phys. **74**, 11 (2002).